Available online at www.sciencedirect.com

ScienceDirect

materialstoday: PROCEEDINGS

Materials Today: Proceedings 2S (2015) S408 – S413

Joint 3rd UK-China Steel Research Forum & 15th CMA-UK Conference on Materials Science and Engineering

Determination of a set of constitutive equations for an Al-Li alloy at SPF conditions

Haoxiang Gao[a], Nan Li[a], Hongliang Ho[b], Yanling Zhang[b], Ning Zhang[b], Liliang Wang[a,*], Jianguo Lin[a]

[a]*Department of Mechanical Engineering, Imperial College London, London SW7 2AZ, United Kingdom*
[b]*Beijing Aeronautical Manufacturing Technology Research Institute, Beijing 100024, China*

Abstract

Uniaxial tensile tests of aluminium-lithium alloy AA1420 were conducted at superplastic forming conditions. The mechanical properties of this Al-Li alloy were then modelled by a set of physicallybased constitutive equations. The constitutive equations describe the isotropic work hardening, recovery and damage by dislocation density changes and grain size evolution. Based on a recent upgraded optimisation technique, the material constants for these constitutive equations were determined

Selection and Peer-review under responsibility of the Chinese Materials Association in the UK (CMA-UK).

Keywords: Al-Li alloy,Superplastic forming, microstructure evolution, damage evolution, constitutive equation

* Corresponding author. Tel.: +44(0)20 7594 3648
E-mail address: liliang.wang@imperial.ac.uk

Selection and Peer-review under responsibility of the Chinese Materials Association in the UK (CMA-UK).
doi:10.1016/j.matpr.2015.05.056

1. Intoduction

Superplasticity is the ability to sustain extensive elongations (more than 200%) without necking and fracture in the fine-grained material[1].The superplastic phenomenon only occurs in a certain range of temperatures and strain rates, which are characterised by low flow stress and high strain rate sensitivity [2]. The mechanism of superplastic deformation includes grain rotation, grain boundary sliding and the fine dispersion of thermally stable particles by pinning the grain boundary within the fine structure. [3]

In recent years, Aluminium Lithium (Al-Li) alloys have become attractive materials for the aerospace and aeronautic industries. With a high specific strength, high stiffness and good fatigue strength, aluminium lithium alloy is regarded as a promising material competing with composite materials [4]. The Al-Li alloy not only provides good mechanical properties that satisfy the requirements in the manufacturing of aero-components, but is also a light weight alloy, because Li has an extremely low density, for each 1wt% addition, the density of the Al alloy can be reduced by 3%, the aero-structural components consisting of the Al-Li alloy offer a great potential for weight reduction. [5]

In the manufacturing of aero-components, superplastic forming (SPF) is an effective forming technique which can produce lightweight components with complex geometries. SPF requires low forming pressure but offers superior capability in forming large-scale complex-shaped components with excellent flexibility in the design and relatively low cost for forming tools. However, the low production rate is one of the technical limitations for SPF, which retards the development of SPF in the high volume industrial production of light weight components [6]. In recent years, finite element (FE) simulations have been widely used in the SPF industry to provide effective guidance for the forming process optimizations and tool design. The reliability of the FE simulation results is determined by the accuracy of the input data, e.g. the material models. Two important aspects of material models should be taken into account. One is to predict the mechanical behaviour accurately. The other one is to represent the evolution of key physical features. For instance, B.H Cheong et al established an integrated numerical step bar model using constitutive equations [7].In their model, the constitutive equations captured the flow stress curves successfully at different strain rates and temperatures. In addition, the grain size gradient as one of the parameters involved in the microstructure evolution was presented, which provided a good prediction of necking in the superplastic material by generating a necking map.

More recently, the development of constitutive equations used in forming simulations tends to concern more physical aspects, such as the material hardening mechanisms [8],which is not only induced by grain growth, but also related to dislocations. Lin and Dean indicated that the recovery, re-crystallization and damage can be modelled by developing the dislocation-based constitutive equations [9].When the material was stretched severely, damage would occur. Previously, B.H Cheong et al have developed a superplastic micro-damage creep model [7]. Based on the study of Cock and Ashby [10], the new model introduced the fundamental theory of damage mechanisms, i.e. inter-granular void growth. Mohamad et al generalised visco plastic-damage constitutive equations to describe the overall damage effects of the material at hot/warm forming conditions [11].

In this study, a physically based model for SPF process was developed which integrated microstructure and damage evolutions together. The set of constitutive equations was determined from experimental tensile test data of AA1420 at 440°C. Flow stress, recovery, grain size evolution and damage evolution were all addressed by this model.

2. SPF visco plastic-constitutive equations with microstructural evolution and damage evolution

2.1. Power law

During the deformation of a ductile alloy, dislocation controlled deformation dominates when the temperature is below $0.4T_m$ (T_m is the melting temperature of the alloy) [12-13]. The material hardening induced by plastic strain can be represented by power law:

$$\sigma = K\varepsilon^n \tag{1}$$

Where σ is the true flow stress, ε is the true strain, K is a material constant and n is the strain hardening exponent.

When the temperature is above $0.5T_m$, the overall mechanism for plastic deformation is thermally activated and thus the viscoplastic behaviours became more pronounced. Therefore, both strain and strain rate hardening should be considered:

$$\sigma = K\varepsilon^n \dot{\varepsilon}^m \tag{2}$$

Where $\dot{\varepsilon}$ is the strain rate and m is the strain rate sensitivity index.

2.2. Power law superplastic material model

The power law superplastic material model can capture the stress-strain curves successfully and is able to describe the multiaxial flow of superplastic materials in the steady state [12]. For multiaxial flow, the Von Mises yield criterion is employed to calculate the effective stress σ .The material hardening induced by grain growth is defined by $\bar{d}^{-\lambda_1}$. The isotropic hardening caused by the pile up of the dislocation is described by R . Both material hardening effects involve the microstructure evolution by considering grain size growth and dislocation evolution. The effective plastic strain rate $\dot{\varepsilon}^p$ is expressed in Eq. 3:

$$\dot{\varepsilon}^{P} = \left(\frac{\sigma - R - k}{K} \right)^{n_c} \cdot \bar{d}^{-\lambda_1} \tag{3}$$

where σ is the flow stress, $\bar{d}$ is the average normalised grain size, n_c is the inverse of the strain rate sensitivity, k is initial yield stress, K , and λ_1 are material constants.

2.3. Isotropic material hardening induced by dislocation

During the material deformation at elevated temperature, the pre-existing and newly generated dislocations become active. In the activated slip plane, grain boundary sliding occurs [14]. The isotropic hardening effects have been quantified by the dislocation density evolution [11], which is expressed by Eq. 4. However, the material deformation at elevated temperatures is complicated. Therefore, in this model, the effects of grain orientation and grain boundary networks are neglected.

$$R = B \cdot \bar{\rho}^{0.5} \tag{4}$$

where R is the isotropic hardening and $\bar{\rho}$ is the normalised dislocation density.

$$\bar{\rho} = \frac{\rho - \rho_i}{\rho_m - \rho_i} \tag{5}$$

In Eq. 5, ρ_i is the pre-existing dislocation density of a material before deformation, and ρ_m is the saturated dislocation density. ρ is the actual dislocation density, while $\rho - \rho_i$ is the newly generated mobile dislocation density induced by material deformation. $\rho_m - \rho_i$ is the maximum dislocation density that can be generated due to material deformation. The normalised dislocation density $\bar{\rho}$ is the ratio between the new generated dislocation density and the maximum dislocation density that can be generated by deformation. At the beginning of deformation, $\rho - \rho_i$, the initial normalised dislocation density is 0. When the dislocations are saturated, the normalised dislocation density is 1.

The changing rate of normalised dislocation density during plastic deformation is expressed by Eq. 6 [9].

$$\dot{\bar{\rho}} = A \cdot \bar{d}^{\psi_0}(1-\bar{\rho}) \cdot \left|\dot{\varepsilon}^P\right| - C \cdot \bar{\rho}^{\gamma_2} \qquad (6)$$

Where $\dot{\varepsilon}^P$ is the plastic strain rate, A, C, ψ_0, γ_2 are material constants.

In Eq. 6, $A \cdot \bar{d}^{\psi_0}\left|\dot{\varepsilon}^P\right|$ represents the dislocation density generated due to plastic deformation. As the plastic deformation continues, the dynamic recovery occurs, which leads to the annihilation of dislocations. In this case, the dynamic recovery is represented by $A \cdot \bar{d}^{\psi_0} \cdot \bar{\rho} \cdot \left|\dot{\varepsilon}^P\right|$. The two terms, $A \cdot \bar{d}^{\psi_0} \cdot \bar{\rho} \cdot \left|\dot{\varepsilon}^P\right|$ and $A \cdot \bar{d}^{\psi_0}\left|\dot{\varepsilon}^P\right|$, are not thermally-activated terms, and the dynamic grain growth effect is expressed by $\bar{d}^{\psi_0}$. The thermally-activated term is expressed by $C \cdot \bar{\rho}^{\gamma_2}$, which represents the static recovery [9].

2.4. Grain growth

Equations to model grain growth are expressed in Eqs. 7 and 8[8]:

$$\dot{\bar{d}} = \alpha_1 \cdot \bar{d}^{-\gamma_0} + \beta_1 \cdot \bar{d}^{-\gamma_1} \cdot \left|\dot{\varepsilon}^P\right| \qquad (7)$$

$$\bar{d} = \frac{d}{d_i} \qquad (8)$$

where $\bar{d}$ is the normalised average grain size, d is the average grain size and d_i is the initial average grain size. $\dot{\varepsilon}^P$ is the plastic strain rate and α_1, β_1, γ_0 and γ_1 are material constants. In Eq. 7, when t=0, d is equal to d_i, and $\bar{d}$ is 1. In Eq. 8, $\alpha_1 \cdot \bar{d}^{-\gamma_0}$ represents the static grain growth effect on average grain size and $\beta_1 \cdot \bar{d}^{-\gamma_1} \cdot \left|\dot{\varepsilon}^P\right|$ is the dynamic grain growth effect on average grain size induced by plastic deformation.

2.5. Damage evolution

The main superplastic deformation mechanisms focus on grain sliding and grain rotation. Both mechanisms can cause void nucleation and growth in the material. Due to the vacancy diffusion, some of the vacancies are localised in the regions around grain boundaries, leading to the nucleation of voids. As the grain boundaries slide, the nucleation and propagation of voids occur in the localised regions due to the stress concentration during deformation. According to the Cocks and Ashby's model, the cavity growth relies on vacancy diffusion. However, it is very complicated to describe the damage model using this diffusion theory at evaluated temperatures and high stress states [10]. In the present research, the superplastic damage equation is considered to be plastic strain dependent, as described in Eq. 9 [11].

$$\dot{\omega} = \beta_4 \cdot \frac{\left|\dot{\varepsilon}^P\right|^{\beta_2}}{(1-\omega)^{\beta_3}} \qquad (9)$$

where ω is damage, $\dot{\varepsilon}^P$ is the plastic strain rate and β_4, β_2, and β_3 are material constants. In Eq. 9, the rate of void growth is a function of plastic strain rate.

2.6. Constitutive equations

$$\dot{\varepsilon}^P = \left(\frac{\left| \frac{\sigma}{1-\omega} \right| - R - k}{K} \right)^{n_c} \cdot \bar{d}^{-\lambda_1} \cdot \frac{1}{(1-\omega)^{\gamma_1}} \quad (10)$$

$$R = B \cdot \bar{\rho}^{0.5} \quad (11)$$

$$\dot{\bar{\rho}} = A \cdot \bar{d}^{\psi_0} (1-\bar{\rho}) \cdot \left| \dot{\varepsilon}^P \right| - C \cdot \bar{\rho}^{\gamma_2} \quad (12)$$

$$\dot{\bar{d}} = \alpha_1 \cdot \bar{d}^{-\lambda_0} + \beta_1 \cdot \bar{d}^{-\psi_1} \cdot \left| \dot{\varepsilon}^P \right| \quad (13)$$

$$\dot{\omega} = \beta_4 \cdot \frac{\left| \dot{\varepsilon}^P \right|^{\beta_2}}{(1-\omega)^{\beta_3}} \quad (14)$$

$$\sigma = E \cdot (1-\omega) \cdot (\varepsilon^T - \varepsilon^P) \quad (15)$$

Due to the presence of damage, an effective stress of $\frac{\sigma}{1-\omega}$ is created to describe its softening effects. Thus, Eq. 3 is modified as Eq. 10, where the term $\frac{1}{(1-\omega)^{\gamma_1}}$ is adopted to provide the equation with higher flexibility. By taking the damage into account in the flow stress-strain relationship, a modified Hooke's Law is given as Eq. 15, where E is the Young's Modulus, ε^P is the plastic strain and ε^T is the total strain.

3. Determination of viscoplasticity-damage constitutive equation

The parameters of the constitutive equations are determined from the uniaxial tensile tests results. The tests were conducted at initial strain rates of 0.01, 0.003, 0.001, 0.0003 and 0.0001s^{-1} at 440 °C. Fig.1 shows the comparison of modelling and experimental results and the predicted flow stress-strain curves are in good agreement with experimental data. The material constants are listed in Table 1.

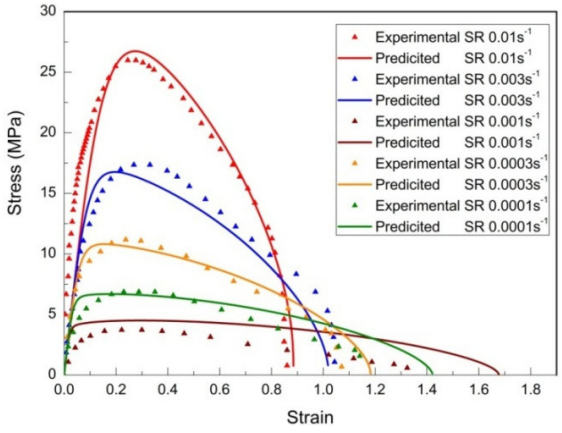

Fig. 1. Comparison of the modelling (solid) and the experimental true stress- true strain curves (symbols) for AA1420 Al-Li alloy at 440°C

Table 1. Optimal material constants of Al-Li alloy at 440°Ccorresponding to Fig.1

K (MPa)	k (MPa)	B (MPa)	α_1	β_1	λ_0	λ_1	ψ_0	ψ_1
220	1E-03	4000	1E-04	0.6	10	1.1	4E-04	0.04
γ_1	γ_2	β_3	β_4	β_2	n_c	A	C	E (MPa)
1.45	2.173	1.265	1.13	1.16	2.30	1E-07	220	195

As shown in Fig.1, the flow stress of AA1420 increases significantly with increasing strain rate, which reflects the pronounced visco-plastic behaviour of the material at SPF conditions. The increase of material strength at higher strain rate was due to strain hardening and grain growth. The ductility of AA1420 decreased with increasing strain rate, because the rate of damage nucleation and growth is faster at higher strain rates. It is worth noting that the flow stress tends to decrease gradually when the strain is over 0.3, which is primarily caused by damage induced softening at high strain level.

4. Conclusions

A set of physically based constitutive equations have been developed for AA1420 Al-Li alloy. The predicted flow stress-strain curves are in good agreement with experimental data. The model accounts for dislocation induced isotropic hardening grain growth induced material hardening and damage evolution. This set of constitutive equations are able to predict the softening effect on the mechanical properties of 1420 Al-Li alloy at high strain level.

Acknowledgements

The strong support from Aviation Industry Corporation of China (AVIC) for this funded research is much appreciated. The research was performed at the AVIC Centre for Structural Design and Manufacture at Imperial College London. The help from Dr. M. Mohamed S K, Mr Omer EL Fakir and Mr Kang Ji are gratefully acknowledged for this conference paper.

Reference

[1] B. R. Grimes R, in: HC Heikkenen, TR Mcnelley (Eds.) The forming behaviour of commercially available superplastic aluminium alloys, the Metallurgical Society, Inc., Warrendale, PA, USA,1988, pp. 97–114.
[2] F. Mohamed., Mater. (Basel). (2011) 1194–1223.
[3] A.K. Mukherjee, Mater.Sci.(1979) 191–217.
[4] R.J.H Wanhill (2014) Aerospace Application of Aluminium-Lithium. In N.E. Prasad, A.A.Gokhale, R.J.H. Wanhill(Eds.), Alum. Alloy.Process. Prop. Application, Elsevier Inc., Oxford, UK, 2014, pp. 506–509.
[5] J. R. Pickens, J.Mater. Sci. 20 (1985) 4247-4258.
[6] a. Barnes, J. Mater. Eng. Perform.,16 (2007) 440–454.
[7] B. H. Cheong, J. Lin, and A.A. Ball, J. Mater. Process. Technol.134 (2003) 10–18.
[8] T.-W. Kim, F. P. E. Dunne, Proc. R. Soc. A Math. Phys. Eng. Sci. 455, (1999) 701–718.
[9] J. Lin *, Y. Liu, D. C. J. Farrugia, M. Zhou, Philos. Mag. 85 (2005) 1967–1987.
[10] G. H. Edward, M. F. Ashby, Acta Metall. 27(1979) 1505-1518
[11] J. Lin, M. Mohamed, D. Balint, T. Dean, Int. J. Damage Mech. 23 (2013) 684–701.
[12] J. Lin, B. H. Cheong, X. Yao, J. Mater. Process. Technol. 125–126 (2002) 199–205.
[13] B. H. Cheong, J. Lin, A.A Ball, J. Strain Anal. Eng. Des. 35 (2000) 149–157.
[14] U. Messerschmidt and M. Bartsch, Mater. Chem. Phys. 81(2003) 518–523.